J. Fluid Mech. (1998), *vol.* 359, *pp.* 329–356. Printed in the United Kingdom

The effects of a favourable pressure gradient and of the Reynolds number on an incompressible axisymmetric turbulent boundary layer. Part 1. The turbulent boundary layer

By H. H. FERNHOLZ AND D. WARNACK

Hermann-Föttinger-Institut für Strömungsmechanik, Technische Universität Berlin, Strasse des 17. Juni 135, 10623 Berlin, Germany

(Received 21 June 1996 and in revised form 4 November 1997)

The effects of a favourable pressure gradient ($K \leqslant 4 \times 10^{-6}$) and of the Reynolds number ($862 \leqslant Re_{\delta_2} \leqslant 5800$) on the mean and fluctuating quantities of four turbulent boundary layers were studied experimentally and are presented in this paper and a companion paper (Part 2). The measurements consist of extensive hot-wire and skin-friction data. The former comprise mean and fluctuating velocities, their correlations and spectra, the latter wall-shear stress measurements obtained by four different techniques which allow testing of calibrations in both laminar-like and turbulent flows for the first time. The measurements provide complete data sets, obtained in an axisymmetric test section, which can serve as test cases as specified by the 1981 Stanford conference.

Two different types of accelerated boundary layers were investigated and are described: in this paper (Part 1) the fully turbulent, accelerated boundary layer (sometimes denoted laminarescent) with approximately local equilibrium between the production and dissipation of the turbulent energy and with relaxation to a zero pressure gradient flow (cases 1 and 3); and in Part 2 the strongly accelerated boundary layer with 'inactive' turbulence, laminar-like mean flow behaviour (relaminarized), and reversion to the turbulent state (cases 2 and 4). In all four cases the standard logarithmic law fails but there is no single parametric criterion which denotes the beginning or the end of this breakdown. However, it can be demonstrated that the departure of the mean-velocity profile is accompanied by characteristic changes of turbulent quantities, such as the maxima of the Reynolds stresses or the fluctuating value of the skin friction.

The boundary layers described here are maintained in the laminarescent state just up to the beginning of relaminarization and then relaxed to the turbulent state in a zero pressure gradient. The relaxation of the turbulence structure occurs much faster than in an adverse pressure gradient. In the accelerating boundary layer absolute values of the Reynolds stresses remain more or less constant in the outer region of the boundary layer in accordance with the results of Blackwelder & Kovasznay (1972), and rise both in the vincinity of the wall in conjunction with the rising wall shear stress and in the centre region of the boundary layer with the increase of production.

1. Introduction

Turbulent boundary layers in a favourable pressure gradient (FPG) exist in wind tunnel contractions and turbine cascades, for example. Since the boundary layer is usually rather thin and separation does not occur, important features of FPG flows can often be determined satisfactorily by Euler-code methods without calculating the boundary layer itself. This may explain the relatively small number of experimental investigations – compared with adverse-pressure-gradient boundary layers (APG) – none of which present complete sets of mean and fluctuating-flow data including skin friction in an axisymmetric flow configuration. Axisymmetric flow ensures small variations between flow quantities measured around the circumference and thus comes closest to a two-dimensional flow if sufficient care is taken to obtain uniform starting conditions.

Two different types of accelerated boundary layers were investigated and are described: in this paper (Part 1) the fully turbulent, accelerated boundary layer (sometimes denoted laminarescent) with approximately local equilibrium between the production and dissipation of the turbulent energy and with relaxation to a zero pressure gradient flow (cases 1 and 3); and in Part 2 (Warnack & Fernholz 1998) the strongly accelerated boundary layer with 'inactive' turbulence, laminar-like mean flow behaviour (relaminarized), and reversion to the turbulent state (cases 2 and 4).

Boundary layer investigations which are related to the cases presented in this paper are those of Patel (1965), Patel & Head (1968), and Blackwelder & Kovasznay (1972). We need not repeat here the extensive surveys of FPG boundary layers by Narasimha & Sreenivasan (1973, 1979) and by Sreenivasan (1980, 1982) and will refer to measurements of other authors in succeeding sections of this paper as appropriate.

In the first part of the investigation FPG boundary layers were investigated which remain turbulent throughout (classified as laminarescent by Schraub & Kline 1965 and as soft laminarization by Narasimha 1983), while showing typical properties of a highly accelerated boundary layer, such as low values of the shape parameter H_{12} – here at about 1.20 – and a sharp decrease of the Reynolds number Re_{δ_2}. The initial Reynolds numbers are moderate ($2500 \leqslant Re_{\delta_2} \leqslant 6000$). In cases 1 and 3 the upstream boundary layer developed under approximately constant streamwise pressure over more than 50 boundary layer thicknesses and may be assumed to be independent of low-Reynolds-number effects (cf. Fernholz & Finley 1996). Low initial Reynolds numbers and an insufficient length of the boundary layer upstream of the onset of the FPG in the existing experiments were two major concerns addressed in the review by Sreenivasan (1982). Further problems have been a lack of near-wall measurements and reliable measurements of the wall shear stress (for comments see Narasimha & Sreenivasan 1973; Sreenivasan 1982). Only in a few cases (Patel 1965; Patel & Head 1968; Badri Narayanan & Ramjee 1969) were skin friction probes used (a surface fence and a heat transfer gange) which were independent of the logarithmic law of the wall. Special attention was devoted therefore to the measurement of mean and fluctuating values of the skin friction and to their higher statistical moments. Comparisons are presented (figure 3) between measurements performed with a surface fence, a wall hot wire, a Preston tube (although valid only in certain regions of the FPG flow) and with oil-film interferometry.

Cases 1 and 3 have most in common with the boundary layers investigated by Patel & Head (1968) and Blackwelder & Kovasznay (1972) as seen from table 1 but Patel & Head (1968) did not measure turbulence quantities and Blackwelder & Kovasznay (1972) had no reliable wall shear stress measurements. Here $H_{12} = \delta_1/\delta_2$ is the shape factor, $Re_{\delta_2} = u_\delta \delta_2/\nu$ the Reynolds number, $K = (\nu/U_\delta^2)(\mathrm{d}u_\delta/\mathrm{d}x)$ the acceleration

	$K_{\max} \times 10^6$	$Re_{\delta_2 S}$	H_{12S}	$Re_{\delta_2 \min}$	$H_{12\min}$	$H_{12\max}$	$Re_{\delta_2 E}$	H_{12E}
Case 1	2.01	2549	1.41	1587	1.24	1.41	2746	1.36
Case 3	1.53	5814	1.37	1665	1.19	1.68	3788	1.35
PH	> 2.5	2100	1.40	700	1.27	1.40	800	1.40
PH		6000	1.34	1200	1.21	1.34	1400	1.25
BK	4.8	2500	1.45	650	1.24	1.78	1900	1.42

TABLE 1. Boundary layer data; PH denotes Patel & Head (1968) and BK denotes Blackwelder & Kovasznay (1972)

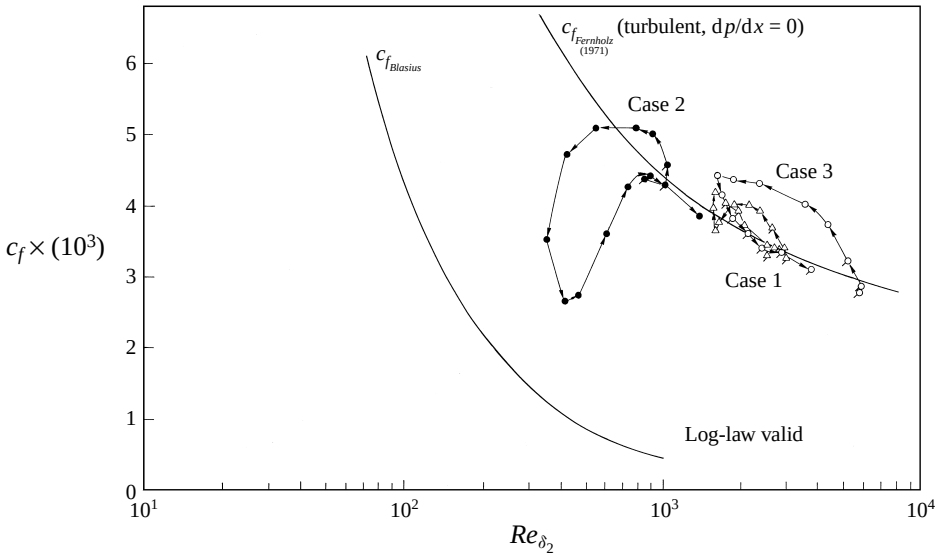

FIGURE 1. Cases 1 to 3 in the (c_f, Re_{δ_2})-plane.

parameter and the indices denote: max for the maximum value, min for the minimum value, S for the starting value and E for the last measuring station.

A further difference between the investigations of Patel & Head (1968) and Blackwelder & Kovasznay (1972) and cases 1 and 3 is that the peak acceleration parameter $K_{\max}$ is larger for the boundary layers of Patel & Head (1968) and Blackwelder & Kovasznay (1972), that the Reynolds numbers at the last measuring station is higher for the present experiments – resulting from a longer relaxation region – and that we present an almost complete set of hot-wire and skin-friction measurements. Cases 1 and 3 are both fully turbulent boundary layers in a favourable pressure gradient and their skin-friction coefficient $c_f = 2\overline{\tau_w}/\rho_\delta u_\delta^2$ lies mainly above the corresponding value at the same Re_{δ_2} for a zero-pressure-gradient (ZPG) boundary layer (figure 1). This is not the case for the relaminarizing boundary layer of case 2 which is also shown for comparison. So this behaviour of the skin-friction coefficient with Reynolds number is characteristic of laminarescent boundary layers such as for cases 1 and 3. The laminarescent boundary layer described here consisted of three regions which show specific features. First, there is an upstream part where the free-stream velocity gradient rises and where the logarithmic law of the wall still holds (local equilibrium between production and dissipation). In the subsequent region the velocity gradient

is both positive and negative and the log law fails. Note that at the location of the breakdown Re_{δ_2} and K differ by a factor of two for case 1 and 3, respectively. Finally, with decreasing acceleration the boundary layer relaxes to its ZPG behaviour and the turbulence structure recovers much faster than downstream from a strong APG.

Besides the mean-flow quantities, this investigation presents the development of the four Reynolds stresses, of some higher moments of the fluctuating velocities and the wall shear stress, of the turbulence production and of the eddy viscosity.

The data give new insight into the physics of the flow and may serve to improve turbulence models which are expected to encounter difficulties in the two turbulent regions – highly accelerated and relaxing – since these are still 'the least understood', (Sreenivasan 1982).

2. Experimental set-up and measuring techniques

The experiments were performed in the low-turbulence wind tunnel (LaWiKa) of the Hermann-Föttinger-Institut. The wind tunnel is a closed-return facility with a centrifugal fan and a 15 kW motor and an additional 1 kW blower to remove the nozzle boundary layer at the start of the test section. The tunnel has a 2 m long axisymmetric nozzle with a 18:1 contraction ratio.

To improve flow uniformity a non-woven filter mat and a single, precisely manufactured, perforated metal plate (64% open area ratio) were mounted at the upstream end of the 2 m diameter settling chamber. The axisymmetric test section (6 m length) consisted of Perspex pipe sections (0.44 m inner diameter) of various lengths, one of which had an elliptical leading edge (6:1) and determined the origin of the test boundary layer on the wall of the test section. The velocity in the empty test section could be varied between zero and $35\,\mathrm{m\,s^{-1}}$ while the mean velocity distribution at the entry was uniform with a deviation from the mean $< 1\%$. The air temperature was kept constant within $\pm 0.1\,^{\circ}\mathrm{C}$.

The favourable pressure distributions were generated by two axisymmetric displacement bodies situated at various positions along the centreline of the test section (figure 2) in order to allow variation of the entry length. The configuration is similar to that of Patel (1965) but in our case the centre bodies were fixed and the probes were positioned along the wall of the axisymmetric test section. The cylindrical displacement bodies were held by radial rods (6 mm in diameter) attached at the rear part so that the boundary layer under examination was not disturbed. The test boundary layer on the wall of the test section was tripped by means of a Velcro tape with a height of 3 mm situated 0.24 m downstream of the leading edge. The turbulence intensity at the inlet to the test section $(\overline{u'^2})^{1/2}/U_{throat}$ was approximately 0.25% and the mean velocity distribution near the inlet was uniform to within $\pm 1\%$. The axisymmetry of the flow was checked by measuring the skin-friction distribution in the circumferential direction, with a Preston tube of 2 mm diameter, at several streamwise locations (figure 25†). The data give the deviations from the value at the respective location of the generator where the profiles were taken and show that, for case 1, the irregularities vary between $+2\%$ and -4% at $x = 2.16$ m and between 0.5% and -3.5% at $x = 4.16$ m.

For successive pressure measurements to be unaffected by small variations in the surface near the pressure tap, by the tube length etc., it is advantageous to use a single

† For reasons of space limits the figures 25 to 27 are in a separate annex available from the JFM Editorial Office.

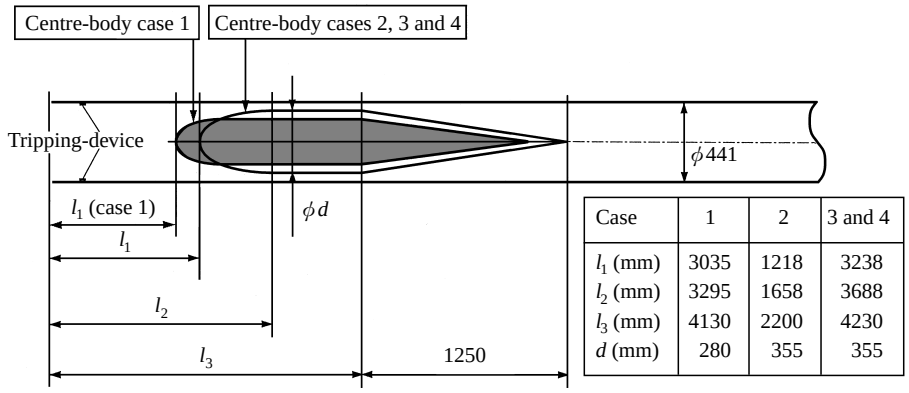

Case	1	2	3 and 4
l_1 (mm)	3035	1218	3238
l_2 (mm)	3295	1658	3688
l_3 (mm)	4130	2200	4230
d (mm)	280	355	355

FIGURE 2. Arrangement of centre bodies for cases 1 to 4.

tap. Therefore, a streamwise slot of 20 mm width was milled along the length of one pipe section and filled with a series of interchangeable plugs; one of these included a static tap (0.70 mm diameter) in its surface and could be positioned every 25 mm along the test wall. The surface of the interchangeable plugs had the same transverse radius of curvature as the pipe to remove the possibility of plug surfaces affecting wall measurements. Static pressure was referenced to that at the inlet, measured with a pressure tap at $x = 246$ mm. For each of the different pressure distributions the free-stream unit Reynolds number at the inlet was kept constant.

The three components of the fluctuating velocity were measured using miniature single and X-wire probes (*uv* and *uw*) with the stem (3 mm diameter) protruding through plugs in the test wall in order to keep the disturbance of the flow as small as possible. The prongs of the crossed-wire probes were mounted at the corners of a square of side length 1.5 mm (see Warnack 1996) and the tungsten/platinum wires, gold plated at the ends, had an active length of 0.55 mm and a diameter of 2.5 μm.

The constant-temperature hot-wire anemometer was an AA – Lab AN – 1003 with the high-frequency option (square-wave-test response in excess of 20 kHz). Data acquisition was achieved using Rhotron hardware controlled by an Atari ST microcomputer. The probes were traversed away from the wall using an electrically driven traverse gear with an incremental resolution of 0.001 mm. Probe access was through an interchangeable plug in the wall of the test section. 30 000 samples (1000 per second) were taken for all velocity measurements. For the wall hot wire the sampling frequency was 250 Hz.

Static pressure was measured using MKS Baratron 220 CD pressure transducers in the ranges 0–100 and 0–1000 Pa and a Prema digital voltmeter 5000 with an integrating multiplexer. For the pressure measurements 60 samples (at a frequency of 1 Hz) were taken for the average value and 120 for the Preston-tube measurements.

Errors in pressure measurements are less than $\pm 0.4\%$, giving the pressure gradient in the highly accelerated region to an accuracy of about 2.5%.

Skin friction was measured by means of Preston tubes, surface fences, wall hot-wire probes, and by oil-film interferometry. The three probes were each integrated into one of the interchangeable plugs described above. The wall hot wires were 0.03 and 0.04 mm away from the wall (Wagner 1991) and the fences had a height of 0.1 and 0.03 mm, respectively. The Preston tubes (diameter between 0.7 and 4 mm) were used with the Patel (1965) calibration curve and served as calibration devices for the surface fence and the wall hot wire. If the Preston-tube measurements are correct within

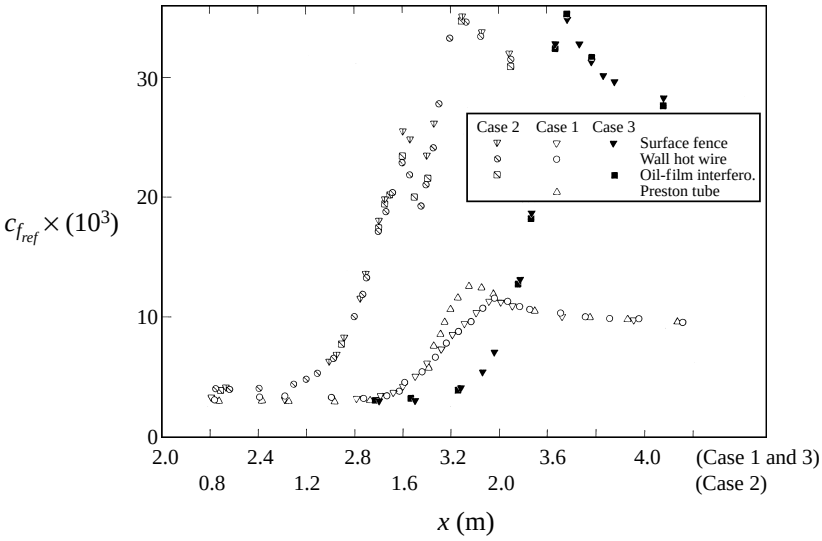

FIGURE 3. Skin-friction distributions measured by four measuring techniques in FPG turbulent boundary layers with (case 2) and without relaminarization (cases 1 and 3).

$\pm 3\%$, the wall hot-wire data should lie within a range of $\pm 4\%$. An additional error source for the hot-wire probes occurs when $\ell^+ > 20$, where $\ell^+ = \ell u_\tau / \nu$ with ℓ as the active wire length, u_τ the skin-friction velocity and ν the kinematic viscosity (see Ligrani & Bradshaw 1987 and Fernholz & Finley 1996, for example).

All wall hot wires had a ratio of active length to diameter of 200 and ℓ^+ never exceeded a value of 28 in case 1 but had higher values in case 3 (see figure 26). Errors caused by high values of ℓ^+ do not affect the mean value of the skin friction but do influence the turbulence level $(\overline{\tau_w'^2})^{1/2}/\overline{\tau}_w$, the skewness $S_{\tau_w'}$ and the flatness $F_{\tau_w'}$. Here the error can lie between 10% and 20%.

Details of the oil-film interferometry method were given by Janke (1992) and Fernholz *et al.* (1996). The determination of the skin friction by this 'absolute' method is estimated to be within $\pm 4\%$.

Since it is known from Patel's early measurements (1965) that the Preston tube fails in a highly accelerated turbulent boundary layer, as a result of the breakdown of the standard logarithmic law, three other methods were used to obtain comparative data. Figure 3 provides this comparison for cases 1, 2 and 3. The skin friction $\overline{\tau}_w$ was made dimensionless with the reference quantity $\rho_\delta u_\delta^2$ measured at $x = 246$ mm, which lies in the ZPG region. Case 1, with the lowest acceleration, shows the breakdown of the Preston-tube method ($\triangle$) in the accelerated flow region whereas the wall-hot-wire ($\circ$) and the surface-fence ($\triangledown$) data collapse onto each other. Case 2, which like case 4 has a highly accelerated flow region with laminar-like flow, shows the departure of the surface-fence data ($\blacktriangledown$) from those of the wall hot wire ($\oslash$) and the oil-film technique ($\boxslash$) in the region around $x \approx 1.65$ m. The breakdown of the Preston-tube method is of course due to the failure of the standard log law. The surface fence must be small enough not to extend beyond the viscous sublayer. It is then not dependent on the logarithmic law. However, it is calibrated for mean values of the skin friction against the mean value of the pressure difference over the fence. Since the behaviour of the system of flow over the fence, tubing, and pressure transducer is nonlinear, a change in the turbulence structure causes a change in the calibration function. One

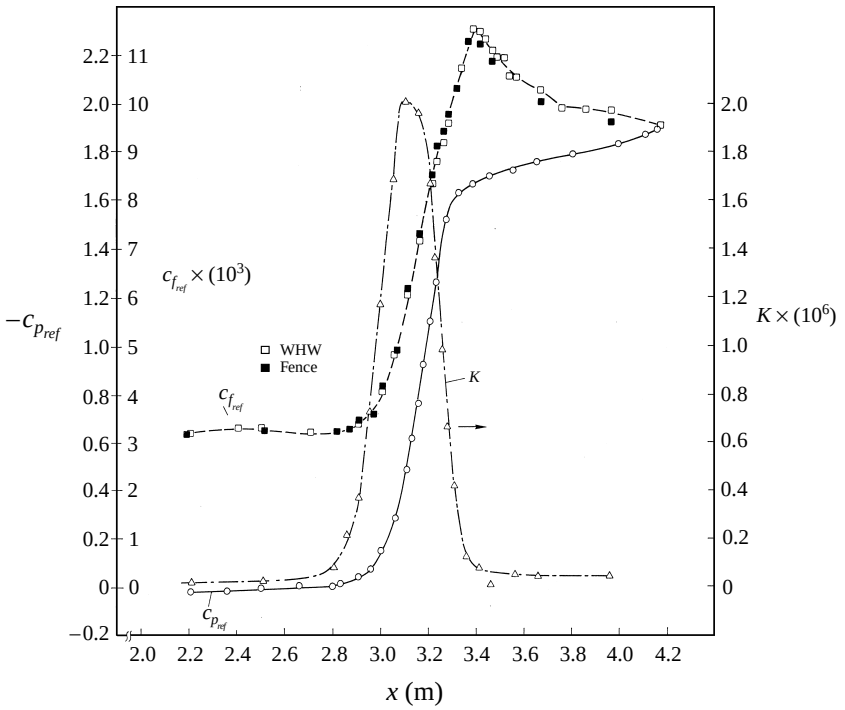

FIGURE 4. Streamwise development of the pressure coefficient $c_{p_{ref}}$, the acceleration parameter K, and the skin-friction coefficient $c_{f_{ref}}$ in a turbulent boundary layer with a favourable pressure gradient (case 1).

criterion for a changed turbulence structure is a change of the skewness $S_{\tau'_w}$ of the shear stress. In the ZPG region where the fence was calibrated $S_{\tau'_w}$ is approximately 1 whereas it reaches a peak value of 3.1 for case 2 at $x = 1.65\,\mathrm{m}$ and here we see the largest difference between the wall-hot-wire and oil-film data. The wall hot wire, however, can resolve the instantaneous value of the wall shear stress and its calibration function for the instantaneous value of the shear stress is independent of the turbulence structure. The mean value can then be determined from the measured time series.

3. Discussion of the mean-flow data

A survey of the development of the FPG turbulent boundary layer (case 1) is presented in figure 4 which shows the streamwise distribution of the static pressure coefficient, $c_{p_{ref}}$, the acceleration parameter, K, and the skin-friction coefficient, $c_{f_{ref}}$:

$$c_{p_{ref}} := \frac{p(x) - p(ref)}{\frac{1}{2}\rho u^2_{\delta_{ref}}}\,, \tag{3.1}$$

$$c_{f_{ref}} := \frac{\overline{\tau}_w(x)}{\frac{1}{2}\rho u^2_{\delta_{ref}}}\,, \tag{3.2}$$

where $p(x)$ is the wall static pressure, $\overline{\tau}_w(x)$ the mean wall shear stress measured by the surface fence (■) or the wall-mounted hot-wire probe (□), $u_{\delta_{ref}}$ is the reference velocity measured by a Pitot-static tube at the reference station $x = 2.208\,\mathrm{m}$, and ρ and ν are the density and the kinematic viscosity, respectively. The pressure p and the

skin friction $\overline{\tau}_w$ in figure 4 were non-dimensionalized by the dynamic pressure at a reference station in the ZPG region to show the full extent of the fall in pressure and of the large increase in skin friction. The acceleration parameter K is plotted in order to facilitate a comparison with other investigations. The displacement, momentum and energy thicknesses are defined for an axisymmetric internal flow as

$$\delta_1 = R-(R^2-2RI_1)^{1/2}; \quad \delta_2 = R-(R^2-2RI_2)^{1/2}; \quad \delta_3 = R-(R^2-2RI_3)^{1/2}; \tag{3.3}$$

with R as the radius of the test section and

$$I_1 := \int_0^\delta \left(1-\frac{\overline{u}}{u_\delta}\right)\left(1-\frac{y}{\delta}\right) \mathrm{d}y, \tag{3.4}$$

$$I_2 := \int_0^\delta \frac{\overline{u}}{u_\delta}\left(1-\frac{\overline{u}}{u_\delta}\right)\left(1-\frac{y}{\delta}\right) \mathrm{d}y, \tag{3.5}$$

$$I_3 := \int_0^\delta \frac{\overline{u}^2}{u_\delta^2}\left(1-\frac{\overline{u}}{u_\delta}\right)\left(1-\frac{y}{\delta}\right) \mathrm{d}y. \tag{3.6}$$

Maximum deviations from the respective definitions for flows along a plane wall were 3.9%, 5.3% and 4.7%. These data show that the corrections made for the axisymmetry of the flow are small.

In the following we shall discuss the development of the above parameters, especially their characteristic values, relate them to the behaviour of other characteristic quantities at these specific locations and then specify certain features of highly accelerated but fully turbulent boundary layers. For an easier comparison with subsequent figures we have marked the flow ranges where the log-law holds and where it fails.

Figures 5(*a*) and 5(*b*) show the streamwise development of the acceleration parameter K, the local skin-friction coefficient c_f, the Reynolds number Re_{δ_2}, and the shape parameter H_{12} for the two boundary layers, respectively. Cases 1 and 3 differ in the peak value of K by a factor of 1.3 with $K_{\max} = 2.01 \times 10^{-6}$, a value below 3.5×10^{-6} beyond that at which relaminarization is found to occur (cf. Sreenivasan 1982). Re_{δ_2} increases from the leading edge of the test section, reaches a maximum at the beginning of the acceleration region and a minimum at the same location as δ_2. The boundary layer and with it Re_{δ_2} grow again with the relaxing acceleration. In the acceleration region the skin friction rises faster than u_δ and so $c_{f_{local}}$ peaks approximately at the end of the acceleration region from whereon the fall of $\overline{\tau}_w$ with almost constant u_δ makes c_f decrease again (case 3, as shown in figure 5*b*). In case 1 (figure 5*a*) the distribution of $c_{f_{local}}$ shows a small double peak pattern which is not seen in figure 4 where $c_{f_{ref}}$ was plotted for the same case. A recheck of the data excludes faulty measurements and we may see here the boundary between a laminarescent boundary layer and one close to the start of relaminarization. In the latter case the decrease of c_f is much larger than for the laminarescent boundary layer (see figures 3 and 4 of Part 2). The shape parameter H_{12} decreases as the boundary layer enters the favourable pressure gradient and reaches a minimum value of 1.24 (case 1) which agrees – accidentally since the peak values of K are different (see table 1) – with the minimum value found by Blackwelder & Kovasznay (1972). Case 3 has a smaller acceleration and a higher initial Re_{δ_2} and consequently only reaches a higher value of the minimum shape parameter ($H_{12\min} = 1.34$). With the same initial Reynolds number as in case 3 but with higher $K_{\max}$ (the actual value is probably larger than 2.5×10^{-6}) Patel & Head (1968) obtain $H_{12\min} = 1.2$. Further downstream H_{12} increases again to the value of that in a ZPG boundary layer as does the skin-friction coefficient. This behaviour is the opposite to that found in

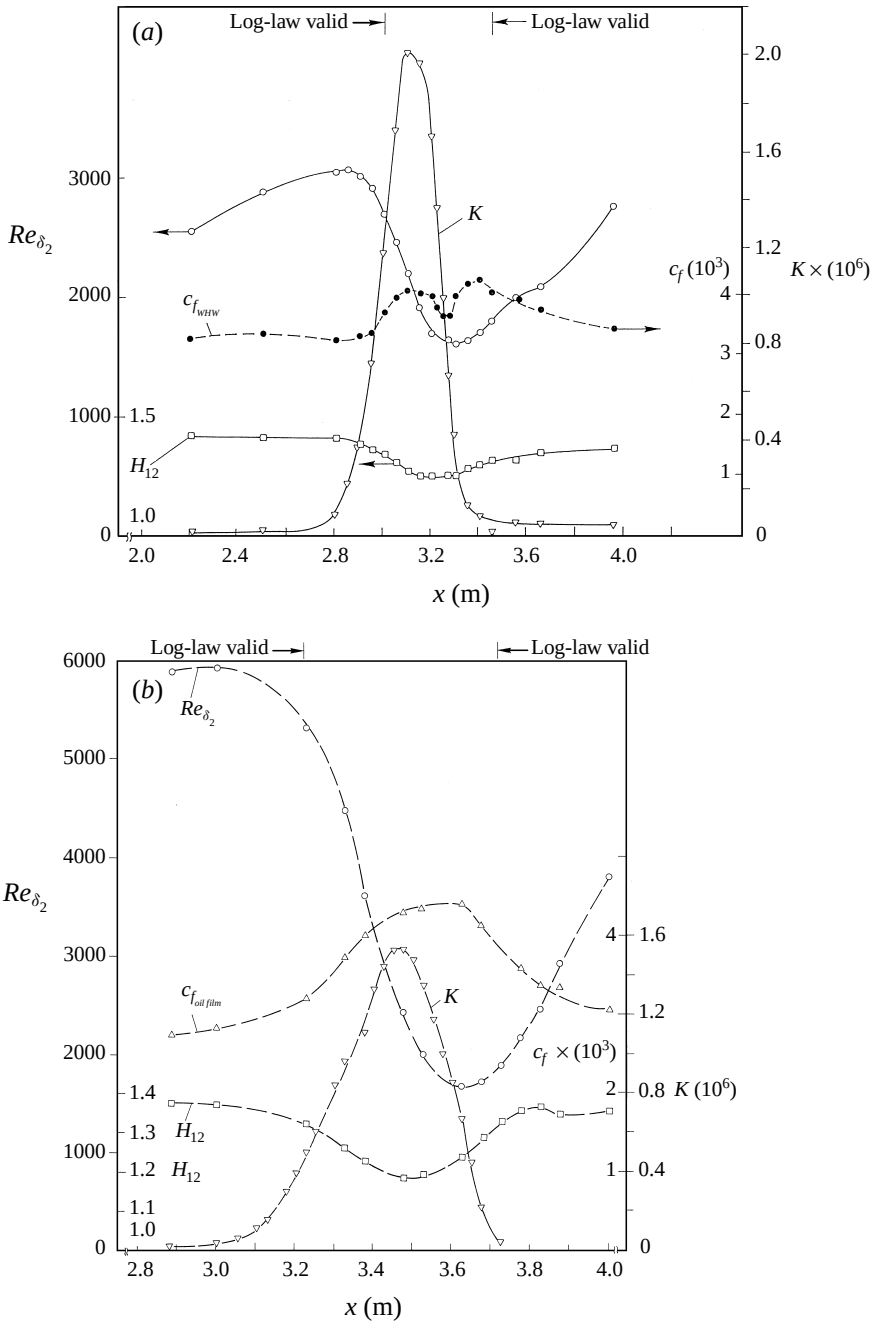

FIGURE 5. Streamwise development of the Reynolds number Re_{δ_2}, the shape parameter H_{12}, the skin-friction coefficient c_f, and the acceleration parameter K in a turbulent boundary layer with a favourable pressure gradient (lines are for visual aid only). (*a*) Case 1. (*b*) Case 3.

a boundary layer downstream of a relaminarization region (see Part 2) where the boundary layer must build up its turbulence structure again and then relaxes to the ZPG conditions. Figures 6(*a*) and 6(*b*) show the mean-velocity profiles in inner-law scaling in comparison with the standard logarithmic law of the wall (the constants

Author	Re_{δ_2}	$K \times 10^6$	$-\Delta_p \times 10^3$	$\Delta_\tau \times 10^6$	$-\beta$	$c_f \times 10^3$	m	H_{12}	H_{32}
Case 1	2685	1.18	16.0	61.6	2.35	3.70	10.9	1.34	1.805
	2442	1.69	20.4	55.6	2.79	3.93	18.5	1.31	1.822
Case 2	1045	1.35	12.5	48.6	0.88	4.57	2.75	1.41	1.784
	924	2.64	21.4	60.5	1.34	5.0	6.58	1.35	1.815
Case 3	5309	0.49	7.9	22.8	3.23	3.22	7.97	1.32	1.806
	4462	0.96	12.5	32.2	3.02	3.73	17.8	1.26	1.838
Case 4	2574	0.11	1.68	15.0	0.25	3.22	0.64	1.41	1.774
	2290	0.13	15.2	50.5	2.07	3.89	8.04	1.38	1.799
PH	1892	0.99	11.7	—	1.08	3.51	—	1.35	—
	1857	2.19	21.0	—	2.42	3.86	—	1.34	—
PH	5179	0.60	9.4	—	2.57	3.05	—	1.32	—
	4446	1.75	21.0	—	5.38	3.18	—	1.29	—
BR	275	3.06	19	—	0.43	5.82	—	1.48	—
	264	5.0	30	—	0.61	6.0	—	1.39	—

TABLE 2. Boundary layer parameters: PH denotes Patel & Head (1968) and BR denotes Badri, Narayanan & Ramjee (1969)

are $k = 0.40$ and $C = 5.10$). The legend of the figures gives the corresponding values of R_{δ_2}, u_τ and x, the latter to facilitate a comparision with figures 4, 5(a) and 5(b). The profiles show good agreement with the log law in the ZPG region upstream and in the mild FPG upstream and downstream of the acceleration region where the boundary layer is characterized by near equilibrium of the production and dissipation (Townsend 1961).

Beginning the discussion of the profiles with case 1 (figure 6a), one finds that with higher acceleration, as marked by low values of Re_{δ_2}, the mean-velocity profiles lie above the straight line. Such a behaviour is also observed in velocity profiles in the late stage of transition where equilibrium has not yet been reached. The departure of the mean velocity distribution from the log law is less pronounced for case 3 where the peak acceleration is smaller but where the dominance of the negative pressure gradient is also confirmed. There are, however, two profiles – denoted by □ in each case – which lie below the standard log law for $y^+ \gtrsim 150$. For this behaviour we have no explanation at present. It is interesting to note that both types of profiles occur at approximately the same values of Re_{δ_2} and H_{12} but at very different values of K as is demonstrated in figure 7 where we have presented three profiles from cases 1, 3 and 4. An obvious question that arises here is whether a parametric criterion for the departure of the mean velocity profile from the standard log law can be established. Table 2 presents the relevant parameters of cases 1 to 4 and respective values from other investigations.

To the parameter K we have added the parameters

$$\Delta_p = \frac{\nu}{u_\tau^3 \rho} \frac{\mathrm{d}p_\delta}{\mathrm{d}x}, \tag{3.7}$$

$$\Delta_\tau = \frac{\nu \alpha}{\rho u_\tau^3} = \frac{\nu}{\rho_\tau^3} \frac{\partial \tau}{\partial y} \tag{3.8}$$

defined by Patel & Head (1968) as well as

$$\beta = \frac{\delta_1}{\bar{\tau}_w} \frac{\mathrm{d}p_\delta}{\mathrm{d}x}, \tag{3.9}$$

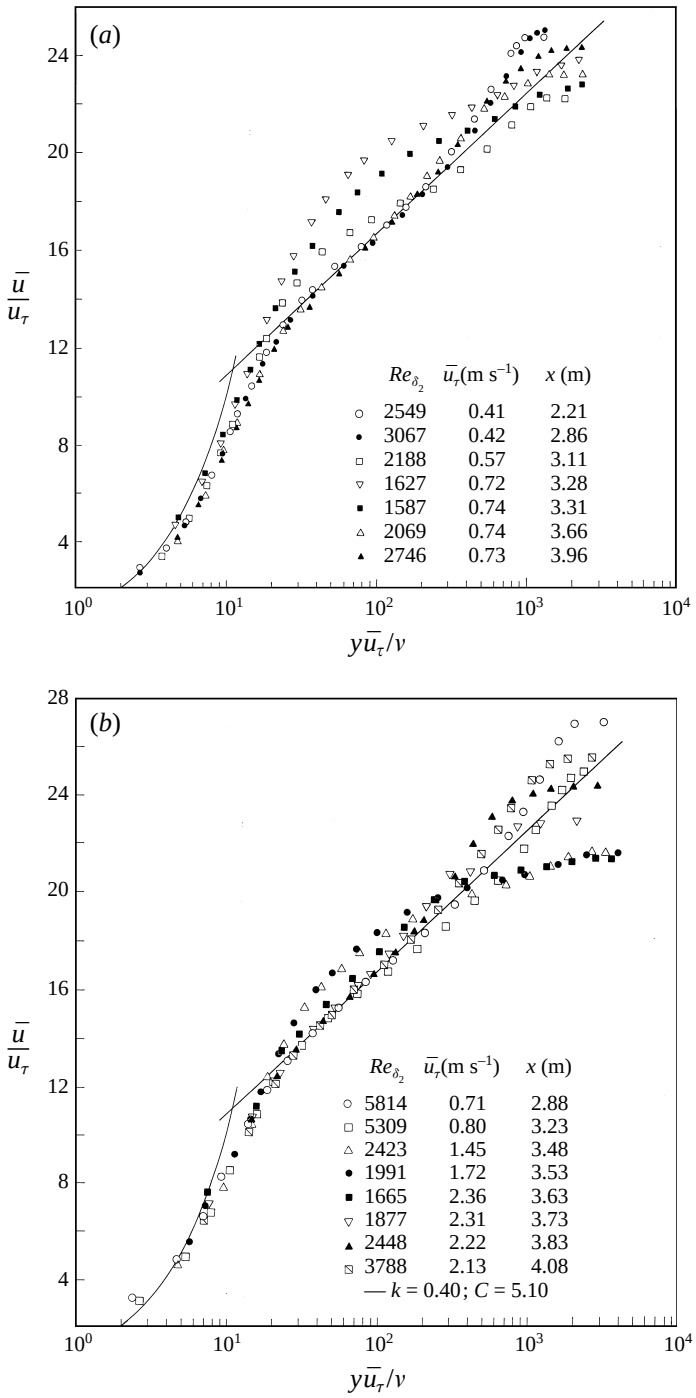

FIGURE 6. Profiles of the mean velocity in inner-law scaling in a turbulent boundary layer with a favourable pressure gradient. (*a*) Case 1. (*b*) Case 3.

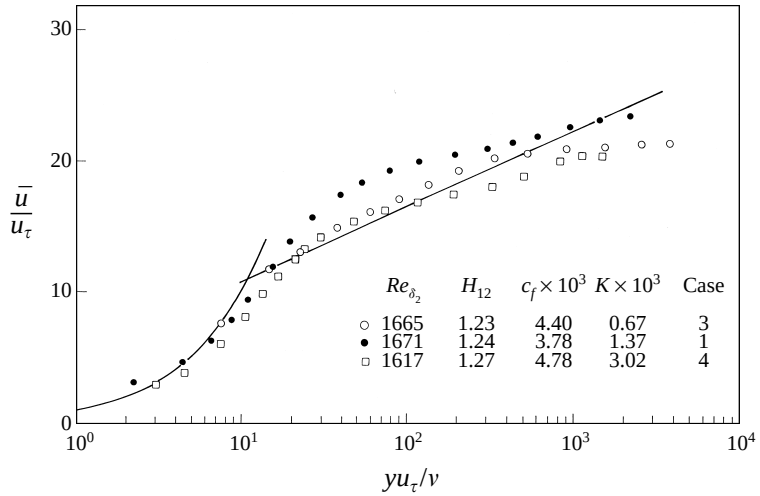

FIGURE 7. Profiles of the mean velocity in inner-law scaling in a turbulent boundary layer with approximately the same Re_{δ_2} and H_{12} but with a different acceleration parameter K.

the shape parameters H_{12} and $H_{32} = \delta_3/\delta_2$ and finally m, defined by

$$m =: (x/u_\delta)\mathrm{d}u_\delta/\mathrm{d}x\,, \tag{3.10}$$

the parameter in the Falkner–Skan equation (e.g. Loitsianski 1967). Comparing the above list of parameters in order to find a criterion for the limit of validity of the log law, only H_{32} shows an approximately constant value which may serve as such a criterion, with $H_{32} \leqslant 1.80$ as an upper limit. This value is independent of Re_{δ_2} in the range investigated but we have no satisfactory physical explanation for its showing this limiting value. Instead we prefer to offer an observation of the changes in other flow properties which occur when the mean profile departs from the standard log law. One of them is the observation that at the same Reynolds number Re_{δ_2} the skin-friction coefficient should reach a value 10% above the value of c_f for a ZPG boundary layer at the same Re_{δ_2} before the profile deviates from the standard log law (figure 1). This criterion holds for $Re_{\delta_2} \gtrsim 1000$.

Another observation concerns changes in characteristic fluctuating quantities (case 1) as shown for example in figure 8. Here we note that the departure from the log law occurs approximately after a 10% decrease of $(\overline{u'^2}/u_\tau^2)_{\max}$ and of $(\overline{\tau_w'^2})^{1/2}/\overline{\tau}_w$ from their respective ZPG levels. Unfortunately we do not have similar data for case 3 but we find the same results for cases 2 and 4 (see Part 2, figure 7).

As for other criteria, Patel & Head (1968) found major departures from the standard log law if their parameter Δ_p reached values of –0.0245. Only cases 1 and 2 approach this value, with –0.020 and –0.021. In cases 3 and 4 Δ_p does not reach more than 50% and 35%, respectively, of the 'critical' value. Δ_p would have been a plausible parameter since it results from the boundary layer equations when non-dimensionalized in inner-law scaling. Figure 9 presents the mean-velocity profiles (case 1) in outer-law scaling, where $\Delta = \delta_1 u_\delta/u_\tau$ is the Rotta–Clauser length. Agreement with the straight line which describes the mean-velocity distribution in a ZPG boundary layer (Fernholz 1969) shows that the upstream profiles follow the ZPG equilibrium behaviour and that the profiles downstream of the acceleration region have not yet fully recovered equilibrium at the last measuring station. This indicates that the velocity distribution

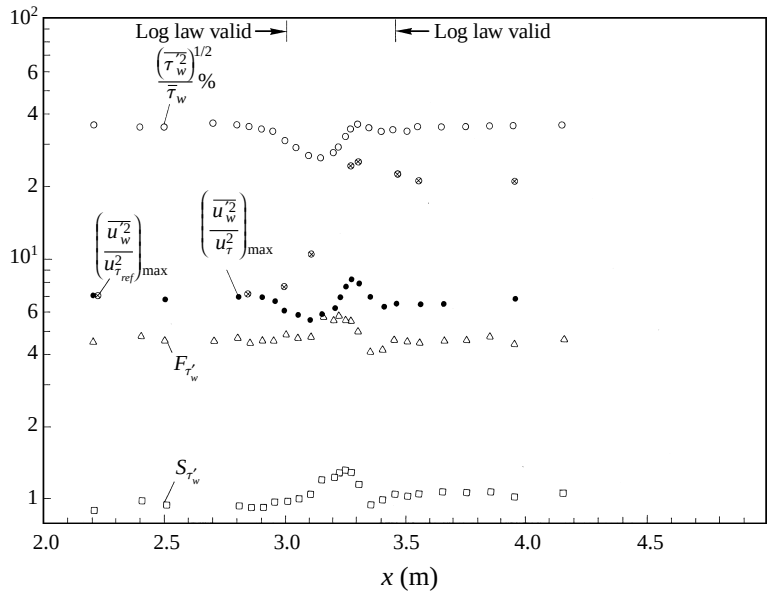

FIGURE 8. Streamwise development of the skin-friction fluctuation, the skewness and the flatness of τ_w', and the maximum value of the dimensionless Reynolds normal stress component in a FPG turbulent boundary layer (case 1).

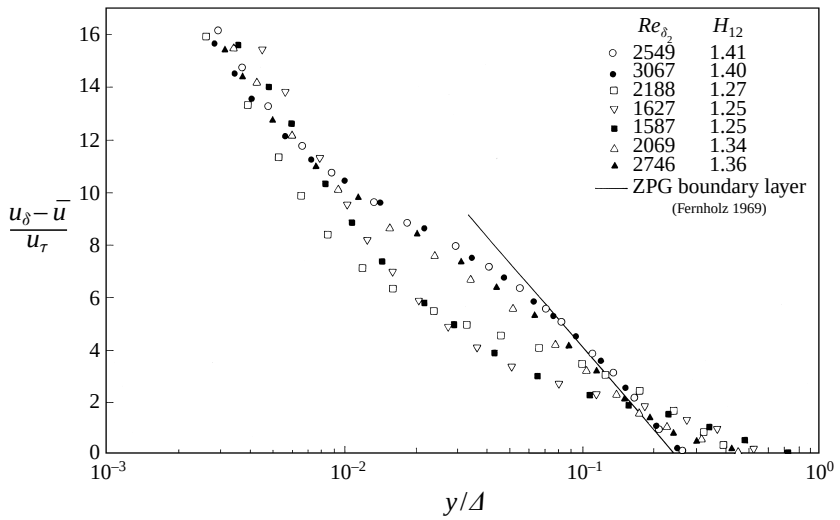

FIGURE 9. Profiles of the mean velocity in outer-law scaling in a FPG turbulent boundary layer. Case 1.

in the outer region returns to equilibrium more slowly than in the inner region (figure 6 *a*) which is consonant with the strong upstream history effects affecting the large structures in the outer region.

4. Discussion of the turbulence data

Turning to the turbulence quantities, one should note that all four components of the Reynolds stress tensor were measured (see Warnack 1996 for details), but only

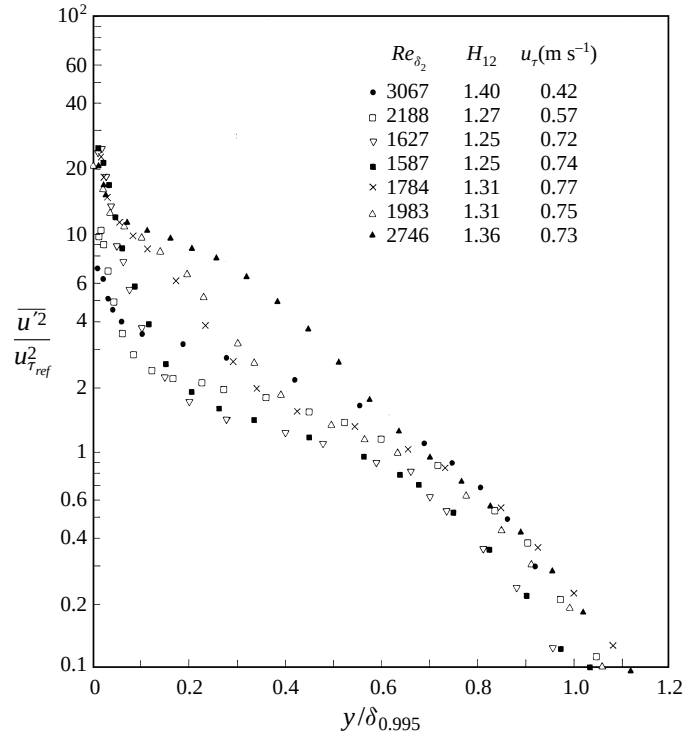

FIGURE 10. Profiles of the Reynolds normal stress component $\overline{\rho u'^2}$ in a FPG turbulent boundary layer (non-dimensionalized by $u_{\tau_{ref}}$). Case 1.

the Reynolds normal stress component $\overline{\rho}\overline{u'^2}$, the Reynolds shear stress $\overline{\rho}\overline{u'v'}$, and the respective production terms $\overline{u'v'}\,\partial\overline{u}/\partial y$ and $\overline{v'^2}\,\partial\overline{u}/\partial y$ will be discussed in detail. Figure 10 presents $\overline{\rho}\overline{u'^2}$–profiles, non-dimensionalized by $\overline{\rho}u_\tau^2$ at the reference station ($x = 2.21$ m), against y/δ in order to show the influence of the FPG on the absolute value of the Reynolds normal stress. Compared with the ZPG reference profile (•), the Reynolds normal stress increases strongly in the near-wall region ($y/\delta \gtrsim 0.1$) in accordance with the rise of u_τ (also observed by Sreenivasan 1982) and remains almost constant in the outer region ($y/\delta > 0.6$) even if the flow is highly accelerated. A distinct change occurs in the centre region where the $\overline{\rho}\overline{u'^2}$-profiles reach a minimum when the mean velocity profiles have their maximum deviation from the standard log law and where both Re_{δ_2} and H_{12} reach their respective minimum. From here on, the $\overline{\rho}\overline{u'^2}$-profiles rise again in the centre region to a level at the last measuring station which is about a factor of 3 higher than for the initial profile. The near-wall behaviour of $\overline{\rho}\overline{u'^2}$ is shown more clearly when the data (case 1) are plotted in inner-law scaling, with the locally defined values of u_τ and v/u_τ (figure 11). The initial fall in the peak value of $\overline{\rho}\overline{u'^2}$ is due to the sharp rise in u_τ but the subsequent strong increase of $\overline{\rho}\overline{u'^2}$ even leads to an overshoot over the initial profile ($Re_{\delta_2} = 3067$). Downstream equilibrium is reached again with decreasing acceleration so that the initial (•) and the end profile (▲) collapse in inner-law scaling. There is no self-similar behaviour of the FPG profiles in the inner region such as can be observed for ZPG boundary layers (e.g. Fernholz & Finley 1996).

For case 3 (figure 26) the peak value of $\overline{u'^2}/u_\tau^2$ falls until Re_{δ_2} reaches its minimum

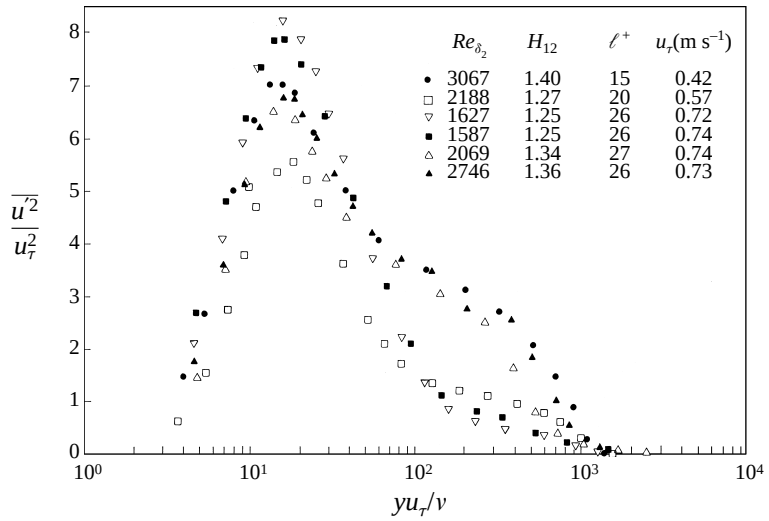

FIGURE 11. Profiles of the Reynolds normal stress component $\overline{\rho u'^2}$ in a FPG turbulent boundary layer. Case 1.

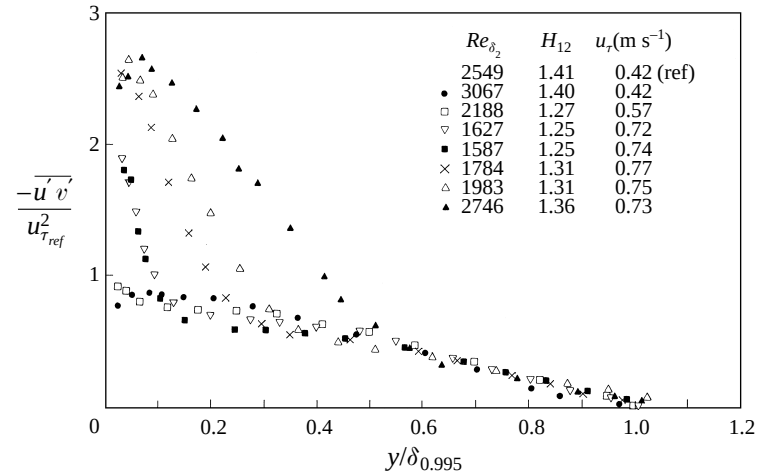

FIGURE 12. Profiles of the Reynolds shear stress $\overline{\rho u'v'}$ in a FPG turbulent boundary layer non-dimensionalized by $u_{\tau_{ref}}$. Case 1.

and then rises again until the end of the measuring region ⧅ without reaching the level of the initial profile (○). The reason for the lower level of $(\overline{u'^2}/u_\tau^2)_{\max}$ may be that the profile had not reached its fully relaxed state or that the high value of the effective length ℓ^+ makes the hot wire see a value which is too low in the wall region (up to 30% according to the data collected by Fernholz & Finley 1996).

The location of the peak values varies little and lies in a range $14 \leqslant y^+_{\max} \leqslant 19$ which is close to $y^+_{\max} \sim 14$, the respective value for a ZPG boundary layer (Fernholz & Finley 1996). This is in contrast to measurements of Blackwelder & Kovasznay (1972) who note that the location of the maximum moves outwards from the wall.

Figure 12 presents the Reynolds shear stress profiles $\overline{\rho u'v'}$ for case 1, non-dimensionalized by $(\rho u_\tau^2)_{ref}$, and plotted against y/δ. The first two profiles show

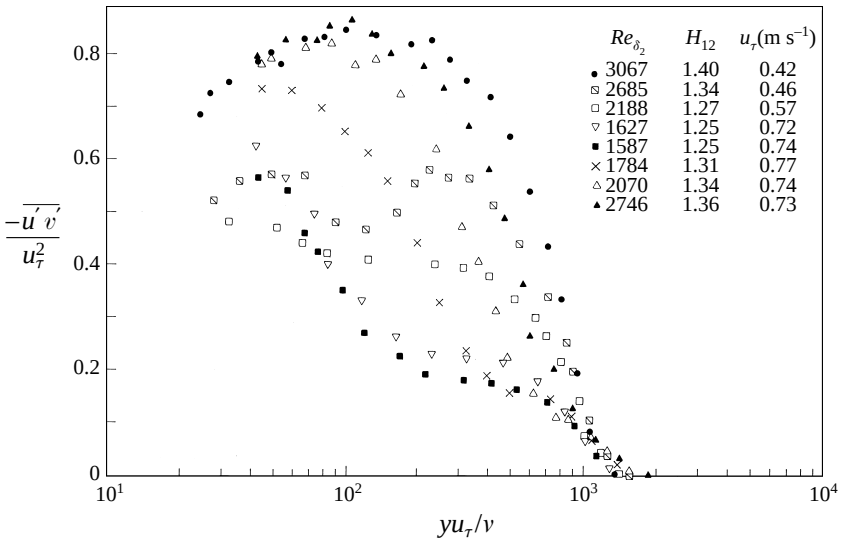

FIGURE 13. Profiles of the Reynolds shear stress $\overline{\rho}\overline{u'v'}$ in a FPG turbulent boundary layer. Case 1.

ZPG-like behaviour in that $(\overline{u'v'}/u_\tau^2)_{\max}$ is approximately 0.9. Then the FPG causes $\overline{\rho}\overline{u'v'}$ to rise sharply in the near-wall region, as the profile adjusts itself to the growth of the wall shear stress. With decreasing acceleration the $\overline{\rho}\overline{u'v'}$-profiles move away from the wall in the centre region of the boundary layer, a process which concurs with the behaviour of the normal stress (figure 10). With the above scaling the Reynolds shear stresses fall on one curve for $y/\delta > 0.55$ independent of the pressure gradient, i.e. they remain practically constant. This is in agreement with the results of Blackwelder & Kovasznay (1972).

In inner-law scaling (figure 13) the same profiles display a different behaviour. Since $\overline{\rho}\overline{u'v'}$ lags behind the growth of u_τ^2, the Reynolds shear stress profiles decrease sharply until the minima of both Re_{δ_2} and H_{12} are reached. Then $\overline{\rho}\overline{u'v'}$ can adjust to the high level of u_τ and comes close to the initial profile. With increasing acceleration the peak of $\overline{u'v'}/u_\tau^2$ not only decreases but shifts by way of an as yet unexplained twin-peak distribution (▨) from the outer region towards the wall. The decline of the outer peak is accompanied by a relative fall of the Reynolds shear stress distribution, with a plateau at about 0.2 (■) at $x = 3.31$ m, the location where $\overline{\tau}_w$ reaches its maximum (figure 4). The near-wall maximum is consequently higher by a factor of three.

Sreenivasan (1982) noted that the excessive thinning of the highly accelerated boundary layer in a laboratory wind tunnel renders the near-wall region almost inaccessible even to miniature X-wires and so measurements of v', w' and $\overline{u'v'}$ are hard to obtain. In the case of the Reynolds shear stress $\overline{\rho}\overline{u'v'}$ this difficulty can be overcome because in a FPG boundary layer the maximum value of the total shear stress τ_t is at the wall and this value can be determined from skin-friction measurements. The distribution of the total shear stress in the near-wall region can then be obtained by, for example, a cubic interpolation curve between the wall shear stress and the last measured values of τ_{total} with $\tau_{total} \approx \overline{\rho}\overline{u'v'}$ far enough away from the wall. From this the molecular shear stress, obtained from near-wall measurements of $\overline{u}$ with a miniature normal hot wire, was subtracted from the interpolated data of τ_t and the Reynolds shear stress determined. Figure 14 shows this extension of

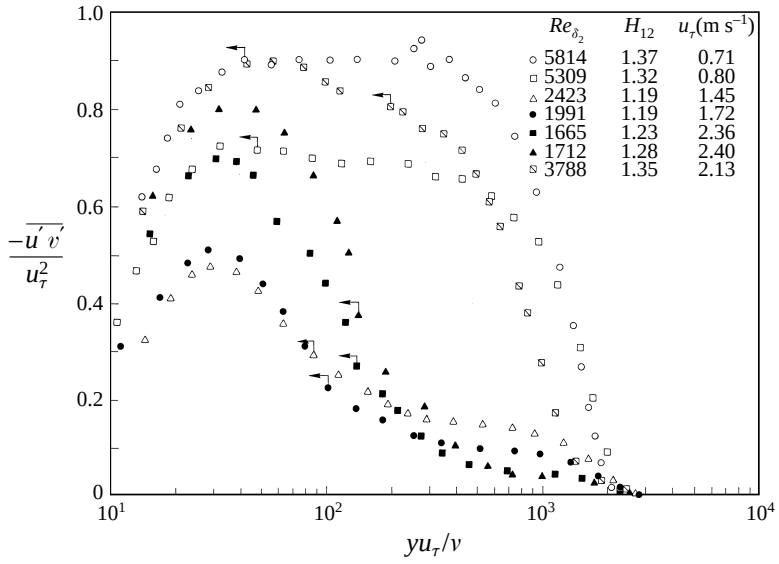

FIGURE 14. Profiles of the Reynolds shear stress $\overline{\rho u'v'}$ in a FPG turbulent boundary layer. Case 3 (← data are extrapolated between this point and the wall).

the near-wall Reynolds shear stress data for the boundary layer with the higher Re_{δ_2} (case 3).

Figures 15 and 27 present the streamwise development of the maxima of all four components of the Reynolds stresses for cases 1 and 3, respectively.

The data points connected by a dashed curve are those measured as close to the wall as possible but are still lower than the actual peak values. They were included because they provide at least a qualitative trend. The curve of the peak value $\overline{u'^2}$ made dimensionless by $(u_\tau^2)_{ref}$ shows a monotonic increase through the acceleration region and a levelling off onto a plateau from above downstream of the acceleration region. This behaviour is characteristic of the distributions $(\overline{u_i'^2}/u_{\tau_{ref}}^2)_{\max}$ for the four Reynolds stresses and can be explained by the higher loss of kinetic energy of the mean flow in a FPG than in a ZPG boundary layer (see Rotta 1962, his equation 8.9.) Normalized with the local u_τ the maximum values of all four components of the Reynolds stress decrease, beginning at the start of the acceleration region ($x \approx 2.80$ m), but this decrease is due to the sharp increase of u_τ only. With decreasing acceleration the Reynolds stresses increase faster than u_τ and their ratios $(\overline{u_i'^2}/u_\tau^2)_{\max}$ reach the initial values again.

In both figures (15 and 27) the validity range of the standard logarithmic law is marked and we note that the departure of the mean-velocity profiles (cf. figures 6*a* and 6*b*) occurs when the peak value of $\overline{u'^2}/u_\tau^2$ falls approximately below 90% of its value for a ZPG boundary layer at the respective Reynolds number. Here we can use the ZPG upstream values as a reference.

The growth of the Reynolds stresses requires a corresponding growth of the turbulence production in the near-wall region as expressed by the two production terms $|\overline{u'v'}|\,\partial\overline{u}/\partial y$ (for the Reynolds normal stress and the turbulent kinetic energy) and $\overline{v'^2}\,\partial\overline{u}/\partial y$ (for the Reynolds shear–stress) in the transport equations.

The production profiles $|\overline{u'v'}|\,\partial\overline{u}/\partial y$ for case 1, made dimensionless by u_τ^3 and the displacement thickness δ_1 (according to Rotta 1962) at the reference station, are

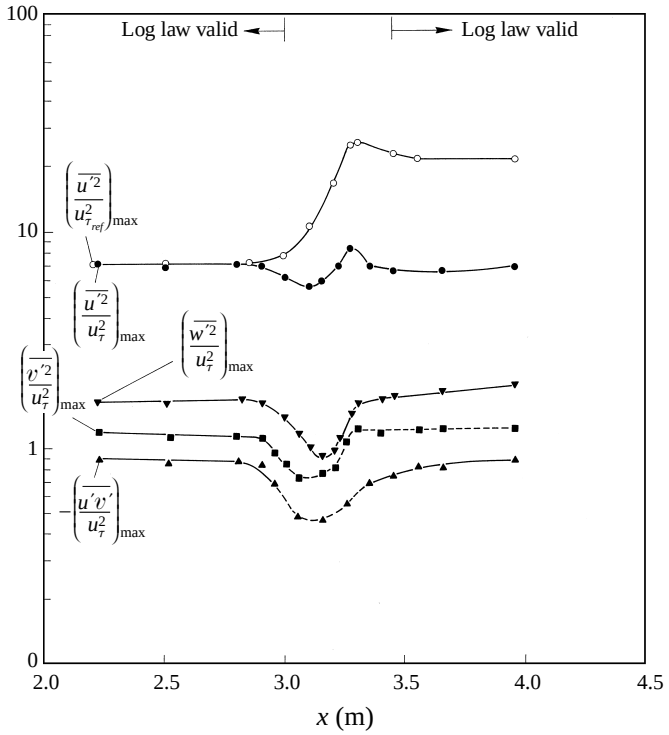

FIGURE 15. Streamwise development of the maxima of the Reynolds stress profiles in a FPG turbulent boundary layer (lines are for visual aid only, the dashed curves connect data points which were those measured nearest to the wall). Case 1.

plotted against y/δ in figure 16 and should be compared with the Reynolds normal stress profiles $\overline{u'^2}/u^2_{\tau_{ref}}$ in figure 10.

Figures 16 and 10 are strikingly similar. We note that the production remains little changed for $y/\delta \gtrsim 0.6$ but that it increases in the inner layer when the acceleration starts and increases in the centre region by about a factor 10 over that of the initial profile at the last measuring station. Since $\overline{u'v'}$ rises only by about a factor 3 (figure 12) in this region, the rise of the production is also caused by an about equal increase of the mean shear $\partial\overline{u}/\partial y$.

Figure 17 shows the profiles of the production term (measured and interpolated $\overline{u'v'}$ data) non-dimensionalized by inner-law quantities u^4_τ/ν and plotted against yu_τ/ν. This scaling shows that the location of the peak value of $[(\nu/u^4_\tau)\overline{u'v'}\,\partial\overline{u}/\partial y]$ is almost independent of Re_{δ_2} in the range $826 \leqslant Re_{\delta_2} \leqslant 5814$ (the data of case 3 are not shown here).

The location of the peak of the production profile corresponds closely with that of the Reynolds normal stress $\overline{\rho}\,\overline{u'^2}$ and lies in the range $13 \leqslant y^+ \leqslant 17$. The height of the peak varies between 0.24 and 0.13 where the smaller values are partly due to the increase of u_τ by a factor of 3. Nevertheless, there is a strong absolute increase of the production term in the near-wall region during the acceleration (figure 16). The production profiles do not show, however, the overshoot which occurred with the Reynolds normal stress profiles (figure 11).

Figure 18 presents the distribution of the production term $\overline{v'^2}\,\partial\overline{u}/\partial y$ for the Reynolds shear stress (case 1), and now figures 18 and 13 correspond very closely with each

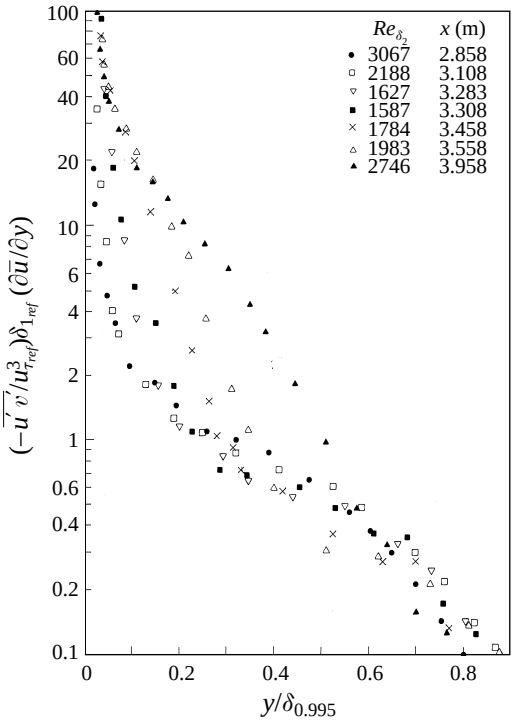

FIGURE 16. Distribution of the production term for the Reynolds normal stress $\overline{\rho u'^2}$ non-dimensionalized by reference quantities ($x = 2.20$ m) in a FPG turbulent boundary layer. Case 1.

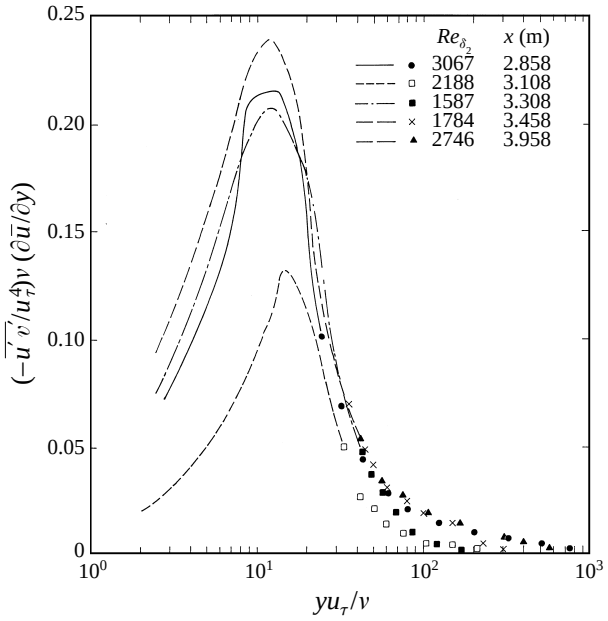

FIGURE 17. Distribution of the production term for the Reynolds normal stress component in a FPG turbulent boundary layer. Case 1 (lines denote extrapolated data).

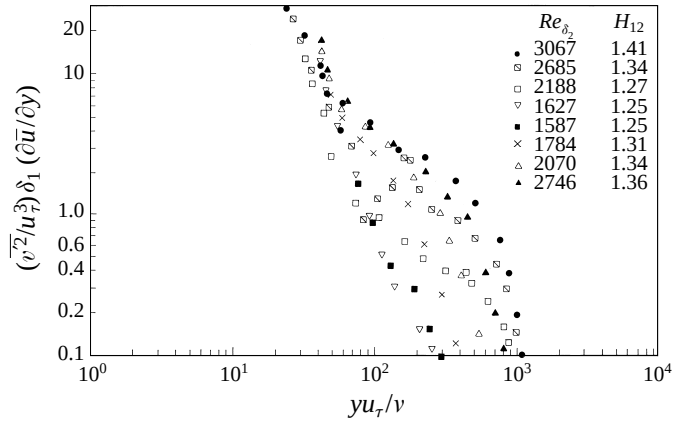

FIGURE 18. Distribution of the production term for the Reynolds shear stress $\overline{\rho u'v'}$ component in a FPG turbulent boundary layer. Case 1.

other, i.e. the production term determines the Reynolds shear stress profile. Note for example the twin-peak configuration (⧅) and the equivalent production profile in the outer layer. The production profiles have in common that their peak is in the inner layer but neither location nor magnitude of the peak could be determined in this case since $\overline{v'^2}$ could not be interpolated in the same manner as $\overline{u'v'}$.

The maximum of the production term $(\overline{u'v'}\,\partial\overline{u}/\partial y)$ is difficult to obtain from measurements, as discussed above, but its value can be calculated. Under the assumptions that the pressure gradient $\mathrm{d}p/\mathrm{d}x$ is zero and that the boundary layer flow in the immediate vicinity of the wall is parallel ($\overline{v}=0$), Rotta (1962, p. 70) derived a simple expression for the maximum of the production term non-dimensionalized in inner-law coordinates for a ZPG boundary layer:

$$\left(\frac{-\overline{u'v'}}{u_\tau^3}\frac{\partial\overline{u}}{\partial y}\frac{\nu}{u_\tau}\right)_{\max}=0.25. \tag{4.1}$$

Taking into account the pressure gradient, it is possible to derive a more general expression which holds for FPG boundary layers and where the assumption of parallel flow is necessary only up to the edge of the buffer layer:

$$\left(\frac{-\overline{u'v'}}{u_\tau^3}\frac{\nu}{u_\tau}\frac{\partial\overline{u}}{\partial y}\right)_{\max}=0.25(1+\Delta_p y_m^+)^2\left(1-\frac{\Delta_p^2A^2}{(1-A\Delta_p)^2}\right) \tag{4.2}$$

where

$$\Delta_p=\frac{\nu}{\rho}\frac{1}{u_\tau^3}\frac{\mathrm{d}p}{\mathrm{d}x},\quad y_m^+=\frac{y_{\max}u_\tau}{\nu},\quad A=\frac{u_\tau^3\rho}{2\nu}\left(\frac{\partial\tau_{mol}}{\partial y}\right)_{\max}. \tag{4.3}$$

The location $y^+_{\max}$ of the production maximum and $(\partial\tau_{mol}/\partial y)_{\max}$ must be obtained from the respective profile or estimated.

A comparison between values calculated from equation (4.2) and the measured maxima of the production term $(\overline{u'v'}/u_\tau^4)\,\nu\,\partial\overline{u}/\partial y$ is shown in figure 19(*a*) and the maxima as a function of the acceleration parameter Δ_p in figure 19(*b*). The agreement is good until the maximum decreases below approximately 0.15 or if Δ_p exceeds about 0.016. For such highly accelerated flows it is no longer possible to neglect the inertia terms in the near-wall region as is appropiate for ZPG and moderately FPG boundary layers.

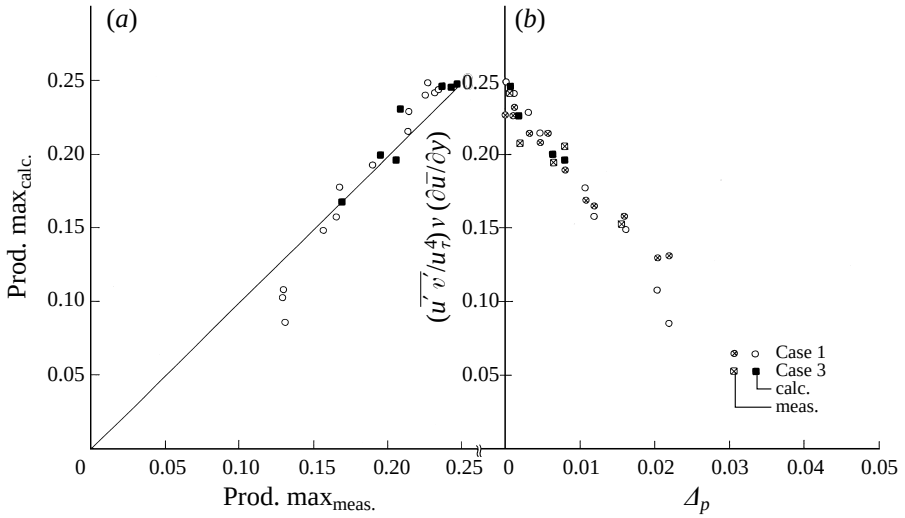

FIGURE 19. (*a*) Comparison between measured and calculated maxima of the production. (*b*) Production maxima plotted against Δ_p (equation (4.2)).

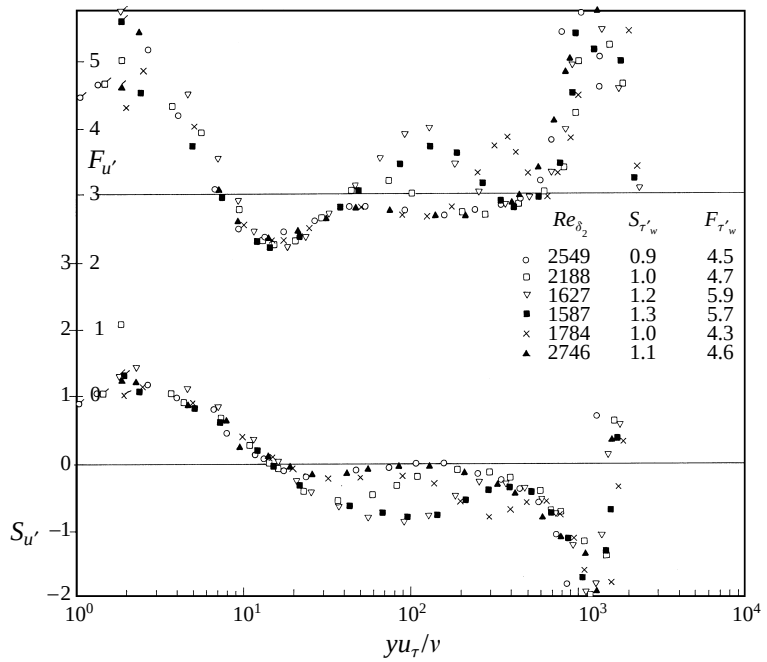

FIGURE 20. Profiles of the skewness S'_u and flatness F'_u in a FPG turbulent boundary layer in inner-law scaling. Case 1 (symbols with a $'$ denote WHW data).

From among the higher moments figures 20 and 21 present the skewness and the flatness of u' in inner-law scaling for cases 1 and 3, respectively. A first inspection shows that the profiles of both cases are qualitatively similar and that there are also similarities with skewness and flatness profiles in ZPG boundary layers (cf. Fernholz & Finley 1996). Figures 20 and 21 show:

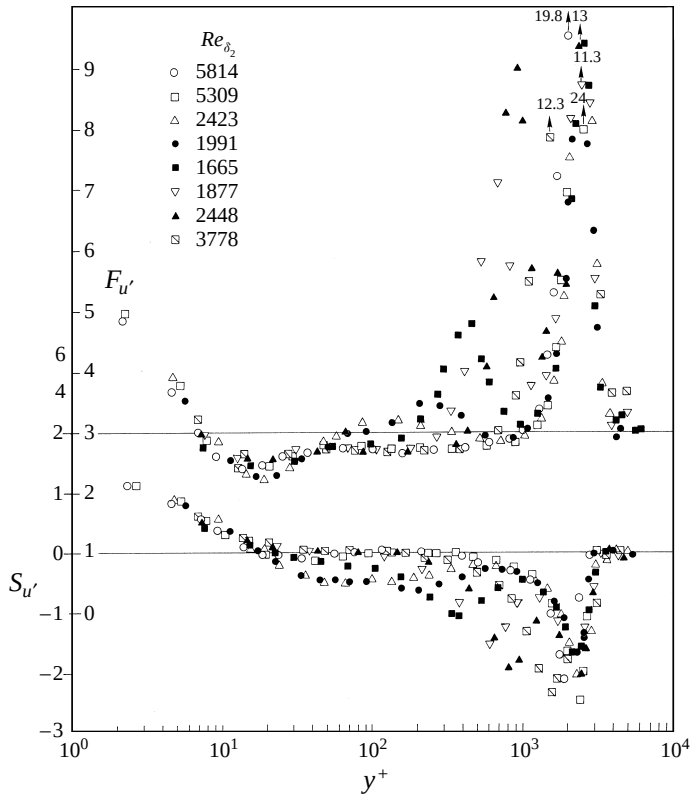

FIGURE 21. Profiles of the skewness S'_u and flatness F'_u in a FPG turbulent boundary layer. Case 3.

(i) independence of the Reynolds number and of the FPG in the viscous sublayer and the buffer layer for the $S_{u'}$ and $F_{u'}$ profiles;

(ii) for the initial ZPG profiles and the profiles relaxing from the acceleration there is also no dependence on Re_{δ_2} in the standard log-law region ($S_{u'} = 0$ and $F_{u'} \sim 2.80$) (see also Fernholz & Finley 1996, their figure 66);

(iii) as with ZPG boundary layers the y^+ position of the maximum of $\overline{u'^2}$, the minimum of $F_{u'}$ and the zero value of $S_{u'}$ coincide within a small range (see the discussion in Fernholz & Finley 1996). This range is within $14 \leqslant y^+ \leqslant 21$, slightly higher than for the ZPG data ($y^+ \approx 14$) in the same Reynolds-number range. This means that the higher moments $S_{u'}$ and $F_{u'}$ are not affected by the FPG in the viscous sublayer and in the buffer layer. Effects do occur, however, in the log-law region where $F_{u'}$ increases by up to 60 % for case 3 (figure 21) before it finally rises to values much larger at the boundary layer edge where they indicate the 'intermittency' between turbulent and non-turbulent periods of the flow. The increase in the log-law region is in accordance with the rise of $\overline{\rho u'^2}$ and the increase of production which we have noticed above. Note that the higher values of $F_{u'}$ are to be found in the boundary layer with the higher Reynolds number.

Wall values for the skewness and flatness for the profiles of case 1 were measured by means of a wall-mounted hot-wire probe and are given in the legend of figure 20. They show an increase of about 30% for both $S_{\tau'_w}$ and $F_{\tau'_w}$ in the region where the acceleration is high and then fall again to the initial values (ZPG). The higher values of the flatness are a measure of an increasing number of events far from the mean

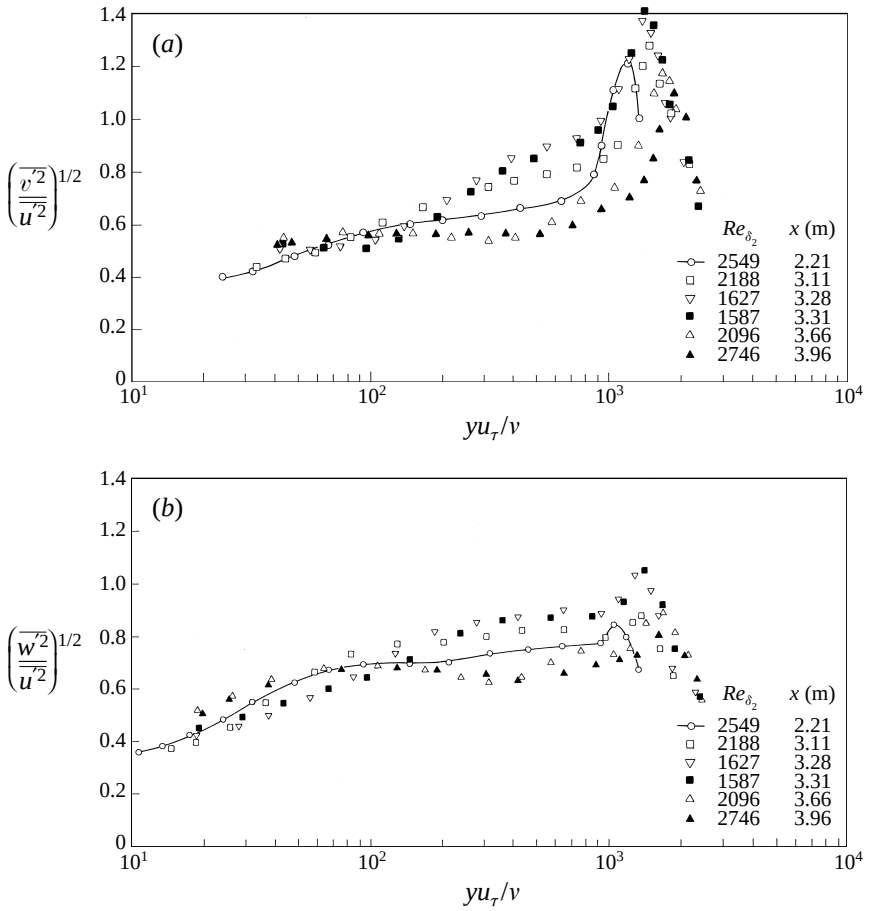

FIGURE 22. Distributions of the anisotropy parameters in a FPG turbulent boundary layer. Case 1. (line is for visual aid only). (*a*) $(\overline{v'^2}/\overline{u'^2})^{1/2}$. (*b*) $(\overline{w'^2}/\overline{u'^2})^{1/2}$.

value which correspond with the increase of the fluctuating component u' and could confirm an increased burst rate.

The behaviour of the turbulence structure affected by the FPG is also shown in the distributions of the structure or anisotropy parameters $(\overline{v'^2})^{1/2}/(\overline{u'^2})^{1/2}$ and $(\overline{w'^2})^{1/2}/(\overline{u'^2})^{1/2}$ in figures 22(*a*) and 22(*b*). Figure 22(*a*) presents the v'-anisotropy with the ZPG distribution (○) dividing the profiles in the acceleration region from those in the recovery region; v'-anisotropy distributions for ZPG boundary layers in the same Re_{δ_2}-range as covered here almost collapse on a single curve (e.g. Fernholz & Finley 1996, their figure 62) and show a distinct peak in the outer region (confirmed by the DNS of J. G. Brasseur 1994, personal communication). The FPG data in figure 22(*a*) are qualitatively similiar but show a slightly higher absolute peak value (1.4 against 1.2) and, for $y^+ > 200$, an increase of v' over u' in the acceleration region and an undershoot in the relaxation region. This suggests that the production of $\overline{\rho}\overline{u'^2}$ is affected by the acceleration before that of $\overline{\rho}\overline{v'^2}$ and that the process is reversed in the relaxation region.

For the w'-anisotropy parameter (figure 22*b*) a comparison with the ZPG case (o) is also possible (e.g. Fernholz & Finley 1996, their figure 64), and the distributions

are again qualitatively similar except for the range $200 < y^+ < 1000$ where one finds an increase and decrease in the acceleration and relaxation region, respectively. The departures from the ZPG case are smaller, since w' can only be changed by redistribution of the energy contents of the components of the fluctuation velocities and not by direct production in a two-dimensional boundary layer.

5. Eddy-viscosity distribution in a laminarescent and a relaminarizing boundary layer

Since eddy-viscosity models still play an important role in numerical calculations of turbulent boundary layers, the present measurements can be used to examine differences in eddy-viscosity distributions of FPG turbulent boundary layers with and without laminar-like states. Comparisons for ZPG and APG were performed by Head (1976) and extended to reattaching wall-bounded shear flows by Johnson, Menter & Rumsey (1994). Previous investigations have concentrated on pressure-gradient effects and neglected the importance of the Reynolds number for the eddy viscosity. We shall therefore discuss the effects of both parameters for a laminarescent and a relaminarizing boundary layer.

Figures 23(*a*) and 23(*b*) show the distribution of the eddy viscosity ν_t made dimensionless by the kinematic viscosity ν and plotted against y^+ in order to emphasize the development in the inner region of the boundary layer for cases 1 and 2 (discussed here rather than in Part 2). The initial profile (ZPG) is denoted by a line to facilitate the discusssion. Peak values which represent absolute maxima here vary between about 25 and 100 with the higher values for the higher Reynolds number, almost independent of the pressure gradient in each case. At the outer edge of the boundary layer the scatter is rather large due to the small values of the quantities and some of the data are omitted.

Inspecting the profiles in the ZPG region ($Re_{\delta_2} = 2549$ and 862) first, one finds them to be self-similar for $y^+ \lesssim 60$ and with the location of the peak moving towards the wall for the smaller Re_{δ_2}. The distributions do not show a clear trend due to the influence of the pressure gradient. The ν_t/ν-profiles reach considerably lower values however (about 50%) when the boundary layer is laminar-like (figure 23*b*). In order to obtain a clearer picture of the relationship between $\nu_{t,\max}$ and the pressure gradient, $\nu_{t,\max}/u_\delta\delta_1$ was plotted against the acceleration parameter K in figure 24 for cases 1 and 2. For $K \to 0$ the peak values agree with those given by Head (1976), i.e. approximately 0.02. With K increasing, the maximum value rises by about 30% up to about $K = 2 \times 10^{-6}$. From here on the increase is stronger but in case 1 the acceleration parameter decreases in the relaxation region whereas K still rises in case 2. So these two flows certainly present a challenge for low-order turbulence models.

6. Discussion

This discussion section deals with items which have not yet been covered by the preceeding sections or need further attention. The first topic deals with the breakdown and recovery of the standard logarithmic law which has been investigated here in an accelerated turbulent boundary layer without relaminarization in the parameter range $K \leqslant 2 \times 10^{-6}$ and with initial Reynolds numbers $Re_{\delta_2} = 2549$ and 5915, respectively. The departure of the mean velocity profile from the log law has been observed earlier (e.g. Patel & Head 1968), and discussed by Sreenivasan (1982), for example, but we still cannot present a parameter criterion (see table 2) for the onset of the departure or

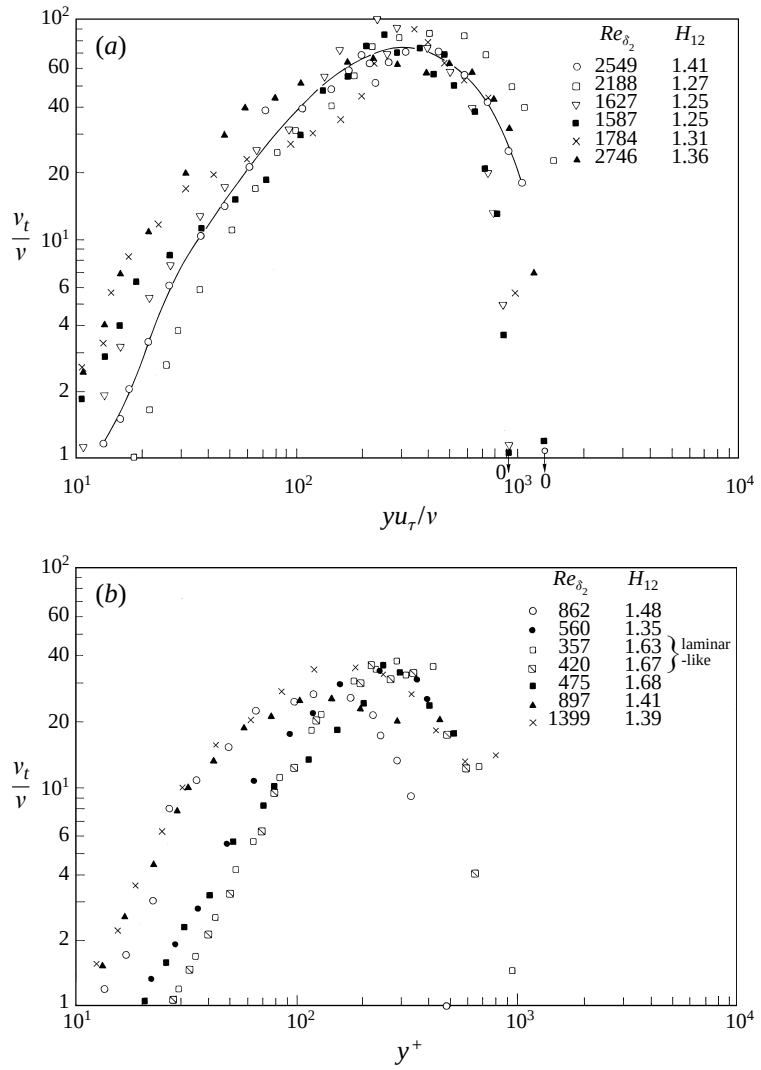

FIGURE 23. Profiles of the dimensionless eddy viscosity v_t/v in a FPG turbulent boundary layer (line is for visual aid only). (*a*) Case 1 (laminarescent). (*b*) Case 2 with relaminarization.

for its end. Since the breakdown of the log law is a gradual process, as has been stated by earlier investigators, we probably should not expect to find such a criterion but should look for changes of turbulence quantities, especially in the near-wall region of the boundary layer. Such quantities are the peak value of the Reynolds normal stress $(\overline{u'^2}/u_\tau^2)_{\max}$ and the ratio of the fluctuating and the mean skin friction $(\overline{\tau_w'^2}/\overline{\tau}_w^2)^{1/2}$. If they are about 10% below their respective ZPG level (here that of the value of the initial profile, e.g. figure 8), the breakdown has occurred. The standard log law holds again downstream of the acceleration region when local equilibrium in the near-wall region is regained, i.e. specifically in the present case when the ZPG condition is reached.

Secondly, a criterion would be useful which could distinguish between highly accelerated boundary layers with and without laminar-like regions. Again we see a gradual process (cf. Narasimha & Sreenivasan 1973) and this is reflected by a

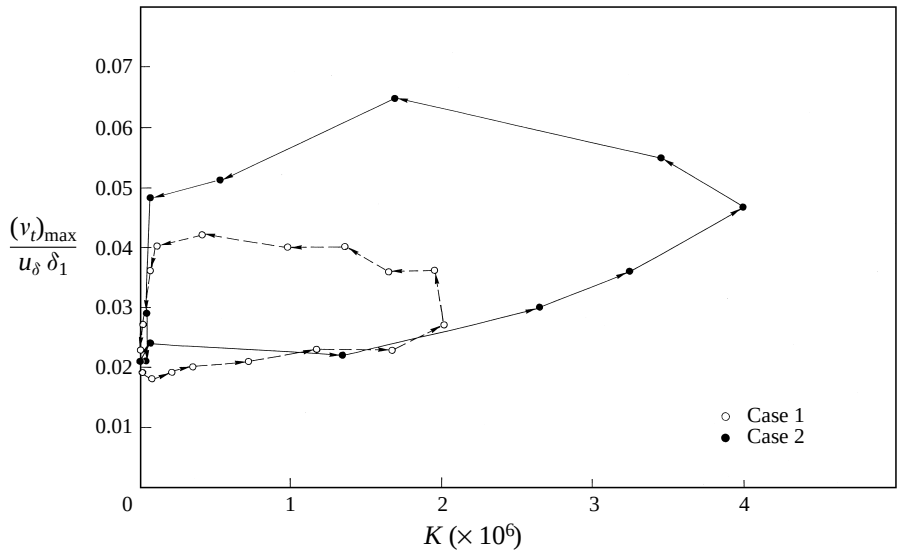

FIGURE 24. Distributions of the peak values of the eddy viscosity v_t in two FPG turbulent boundary layers with and without relaminarization.

range of the pressure gradient parameter $K \gtrsim 3 \times 10^{-6}$. Such a criterion is certainly dependent also on the initial Reynolds number of the boundary layer concerned. The present measurements suggest that a possible criterion for the occurrence of conditions favourable to relaminarization could be the 'short' double peak pattern in the developement of the skin-friction coefficient c_f (e.g. figure 5*a*). This does not occur in case 3 where the boundary layer is less strongly accelerated. But both fully turbulent accelerated boundary layers appear to be characterized by $K_{\max}$, $c_{f_{\max}}$ and $H_{12_{\min}}$ coinciding at about the same x–position (figures 5*a* and 5*b*) with the lowest value $(H_{12})_{\min} = 1.19$ at $Re_{\delta_2} = 2423$.

The last phenomenon to be discussed is the relaxation process downstream of the acceleration region. Here we have a case where a change in pressure gradient is imposed which is both large and rapid (Smits & Woods 1985). Since there is no consensus as to what is a large and rapid change in pressure gradient nor where the relaxation of the turbulence structure from this pressure gradient begins, both can only be defined for each specific case. For cases 1 and 3 we present the peak value of $K_{\max}$ and values of K_S and K_E at the start and the end of the acceleration region, respectively, with δ_S as the 0.995 boundary layer thickness at the location of K_S; $\Delta x_{SE}/\delta_S$ then provides a characteristic length ratio for the acceleration region of about 15 (table 6).

The maximum relaxation length available in the present experiments is determined by the distance Δx_R between the location where Re_{δ_2} has its minimum and the last measuring station. δ_O is the boundary layer thickness at $Re_{\delta_2 \min}$.

Since effects produced by a pressure gradient are felt more rapidly near the wall than in the outer layer (e.g. Smits & Woods 1985), the relaxation process downstream of the pertubation should be felt more quickly in the near-wall region than in the outer region. For the mean velocity profile this would mean that the standard log law has recovered first (figure 6*a*), before the profile has adjusted itself to the outer law (figure 9). Figures 6(*a*) and 6(*b*) show that the mean profile follows the log law approximately after $13\delta_O$ and $6\delta_O$, respectively. The Reynolds stresses should adjust

Case	δ_S(mm)	Δx_{SE}(mm)	$\frac{\Delta x}{\delta_S}$	$K_S \times 10^6$	$K_{\max} \times 10^6$	$K_E \times 10^6$	δ_O(mm)	Δx_R(mm)	$\frac{\Delta x}{\delta_O}$	$Re_{\delta_2 \min}$
1	42.0	600	14.3	0.08	2.01	0.08	26.7	650	24	1587
3	44.4	700	15.8	0.04	1.53	0.03	14.7	450	30.6	1665

TABLE 3

themselves more slowly with the recovery growing outwards. This can be seen in figures 10 and 13 where neither the $\overline{\rho u'^2}$- nor the $\overline{\rho u'v'}$-profiles have quite reached equilibrium in the outer layer at the last measuring station.

7. Concluding remarks

This paper presents the results of an investigation of the effect of a favourable pressure gradient ($K \leqslant 2 \times 10^{-6}$) on the mean and fluctuating quantities of two fully turbulent (laminarescent) boundary layers. The initial Reynolds number upstream of the acceleration region was $Re_{\delta_2} = 2549$ and 5915, respectively. In both cases turbulence played an active role throughout and laminar-like profiles – as described in the companion paper (Part 2) – were not observed. The acceleration was, however, strong enough to cause a breakdown of the standard logarithmic law (see e.g. Patel & Head 1968). None of the criteria for this breakdown presented in earlier references could be confirmed and instead changes of the maximum value of the Reynolds normal stress $(\overline{u'^2}/u_\tau^2)^{1/2}$ and of $(\overline{\tau_w'^2}/\overline{\tau}_w^2)^{1/2}$ about 10% below their respective ZPG level are more suitable indicators of this gradual breakdown. Other characteristic features of highly accelerated turbulent boundary layers without relaminarization are the coinciding of $K_{\max}$, $c_{f\max}$ and $H_{12\min}$ at about the same x-position (figures 5*a* and 5*b*). The relaxation length downstream from the acceleration region was long enough to re-establish the log–law and for the mean flow and the turbulence structures to return almost to ZPG equilibrium conditions.

The distribution of the non-dimensionalized maxima $(\overline{u_i'u_j'}/u_\tau^2)_{\max}$ of the Reynolds stresses shows a plateau–valley–plateau formation in the streamwise direction indicating that the mean wall shear stress rises much more strongly than the peak Reynolds stress in the FPG boundary layer (figures 15 and 27). The range of the fall and rise of the respective peak values coincides with the range where the standard log law breaks down.

The distributions of the non-dimensional production term (figures 16 and 17) explain the behaviour of the Reynolds normal stress (figures 10 and 11) in the FPG region. The maximum of the production term can be calculated if the parameter Δ_p, the position of the maximum $y^+_{\max}$ – which varies between 12 and 18 in cases 1 and 3 – and an additional correction term A (see equation (4.3)) are known. The skewness $S_{u'}$ and flatness $F_{u'}$ distributions resemble those in a ZPG-boundary layer (e.g. Fernholz & Finley 1996) except in the highly accelerated region where, in the range $30 \leqslant y^+ \leqslant 130$, $S_{u'}$ is negative (reaching values as low as -1) and $F_{u'}$ is larger by about 60% (figure 20). In case 3, where the Reynolds number is higher than in case 1, the flatness shows very elevated values in the outer region of the boundary layer (figure 21). Finally the eddy viscosity profiles are presented showing that the challenge for turbulence modelling will probably lie more in the relaxation region downstream of $K_{\max}$ than in the range where K increases steadily.

The second author thanks DFG for financial support of this investigation.

REFERENCES

Badri Narayanan, M. A. & Ramjee, V. 1969 On the criteria for reverse transition in two-dimensional boundary layer flow. *J. Fluid Mech.* **35**, 225–241.

Blackwelder, R. F. & Kovasznay, L. S. G. 1972 Large-scale motion of a turbulent boundary layer during relaminarization. *J. Fluid Mech.* **53**, 61–83.

Fernholz, H. H. 1969 Geschwindigkeitsprofile, Temperaturprofile und halbempirische Gesetze in kompressiblen turbulenten Grenzschichten bei konstantem Druck. *Ing. Arch.* **38**, 311–328.

Fernholz, H. H. 1971 Ein halbempirisches Gesetz für die Wandreibung in kompressiblen turbulenten Grenzschichten bei isothermer und adiabater Wand. *Z. Angew. Math. Mech.* **51**, T 148–149.

Fernholz, H. H. & Finley, P. J. 1996 The incompressible zero-pressure-gradient turbulent boundary layer – an assessment of the data. *Prog. Aero. Sci.* **32**, 245–311.

Fernholz, H. H., Janke, G., Schober, M., Wagner, P. M. & Warnack, D. 1996 New developments and applications of skin-friction measuring techniques. *Meas. Sci. Technol.* **7**, 1396–1409.

Head, M. R. 1976 Eddy viscosity in turbulent boundary layers. *Aeronaut. Q.* **XXVII**, 270–276.

Janke, G. 1992 Über die Grundlagen und einige Anwendungen der Ölfilminterferometrie zur Messung von Wandreibungsfeldern in Luftströmungen. PhD thesis, Technische Universität Berlin.

Johnson, D. A., Menter, F. R. & Rumsey, C. L. 1994 The status of turbulence modeling for external aerodynamics. *AIAA Paper* 94–2226.

Ligrani, P. M. & Bradshaw, P. 1987 Spatial resolution and measurement of turbulence in the viscous sublayer using subminiature hot-wire probes. *Exps. Fluids* **5**, 407–417.

Loitsianski, L. G. 1972 *Laminare Grenzschichten.* Akademie Verlag Berlin.

Narasimha, R. 1983 Relaminarization – magnetohydrodynamic and otherwise. *Prog. Astronaut. Aeronaut.* **84**, 30–52.

Narasimha, R. & Sreenivasan, K. R. 1973 Relaminarization in highly accelerated turbulent boundary layers. *J. Fluid Mech.* **61**, 417–447.

Narasimha, R. & Sreenivasan, K.R. 1979 Relaminarization of fluid flows. *Adv. Appl. Mech.* **19**, 221–309.

Patel, V. C. 1965 Calibration of the Preston tube and limitations on its use in pressure gradients. *J. Fluid Mech.* **23**, 185–208.

Patel, V. C. & Head, M. R. 1968 Reversion of turbulent to laminar flow. *J. Fluid Mech.* **34**, 371–392.

Rotta, J. C. 1962 Turbulent boundary layers in incompressible flow. *Prog. Aeronaut. Sci.* **2**, 1–220.

Schraub, F. A. & Kline, S. J. 1965 A study of structure of the turbulent boundary layer with and without longitudinal pressure gradients. *Rep.* MD-12. Thermosci. Div. Stanford Univ., Stanford.

Smits, A. J. & Woods, D. H. 1985 The response of turbulent boundary layers to sudden perturbations. *Ann. Rev. Fluid Mech.* **17**, 321–358.

Sreenivasan, K. R. 1980 A guide to the data in relaminarizing flows. Report prepared for the 1980–1981 *AFOSR–HTM Stanford Conference On Complex Turbulent Flows.*

Sreenivasan, K. R. 1982 Review article: laminarescent, relaminarizing and retranstional flows. *Acta Mech.* **44**, 1–48.

Townsend, A. A. 1961 Equilibrium layers and wall turbulence *J. Fluid Mech.* **11**, 97–120.

Wagner, P. M. 1991 The use of near-wall hot-wire probes for time-resolved skin-friction measurements. In *Advances in Turbulences* pp. 524–529. Springer.

Warnack, D. 1996 Einige Eigenschaften beschleunigter turbulenter Wandgrenzschichten. Dissertation, TU Berlin.

Warnack, D. & Fernholz, H. H. 1998 The effects of a favourable pressure gradient and of the Reynolds number on an incompressible axisymmetric turbulent boundary layer. Part 2. The boundary layer with relaminarization. *J. Fluid Mech.* **359**, 357–381.